

# Probing the electrostatic aggregation of nanoparticles with oppositely charged molecular ions

Jianxiang Huang<sup>1</sup>, Damiano Buratto<sup>1</sup>, and Ruhong Zhou<sup>1</sup>

<sup>1</sup>Zhejiang University

November 21, 2022

## Abstract

The co-assembly of charged nanoparticles with oppositely charged molecular ions has emerged as a promising technique in the fabrication of nanoparticle superstructures. However, the underlying mechanism behind these molecular ions in mediating the repulsion between these charged nanoparticles remains elusive. Herein, coarse-grained molecular dynamics simulations are used to elucidate the effects of valency, shape and size of molecular anions on their co-assembly with gold nanoparticles coated with positively charged ligands. The findings suggest that the valency, shape and size of molecular anions significantly influence the repulsion and aggregating dynamics among these positively charged nanoparticles. Moreover, the free energy calculations reveal that ring-shaped molecular anions with higher valencies and larger sizes are more effective at reducing the repulsion between these gold nanoparticles and thus enhance the stability of the aggregate. This study contributes to a better understanding of the critical roles of valence, shape and size of ions in mediating the electrostatic co-assembly of nanoparticles with oppositely charged ions and it also guides the future design of DNA templates and DNA origami in co-assembly with oppositely charged nanoparticles.

## Probing the electrostatic aggregation of nanoparticles with oppositely charged molecular ions

Jianxiang Huang<sup>1</sup>, Damiano Buratto<sup>1</sup>, Ruhong Zhou<sup>1,2\*</sup>

<sup>1</sup>Institute of Quantitative Biology, College of Life Sciences, Hangzhou 310027, China

<sup>2</sup>Department of Chemistry, Columbia University, New York, NY10027, USA

\*Correspondence should be addressed [torhzhou@zju.edu.cn](mailto:torhzhou@zju.edu.cn)

## Abstract

The co-assembly of charged nanoparticles with oppositely charged molecular ions has emerged as a promising technique in the fabrication of nanoparticle superstructures. However, the underlying mechanism behind these molecular ions in mediating the repulsion between these charged nanoparticles remains elusive. Herein, coarse-grained molecular dynamics simulations are used to elucidate the effects of valency, shape and size of molecular anions on their co-assembly with gold nanoparticles coated with positively charged ligands. The findings suggest that the valency, shape and size of molecular anions significantly influence the repulsion and aggregating dynamics among these positively charged nanoparticles. Moreover, the free energy calculations reveal that ring-shaped molecular anions with higher valencies and larger sizes are more effective at reducing the repulsion between these gold nanoparticles and thus enhance the stability of the aggregate. This study contributes to a better understanding of the critical roles of valence, shape and size of ions in mediating the electrostatic co-assembly of nanoparticles with oppositely charged ions and it also guides the future design of DNA templates and DNA origami in co-assembly with oppositely charged nanoparticles.

## KEYWORDS

## 1 | INTRODUCTION

The dynamic nature of the self-assembly of charged nanoparticles mediated by crucial interactions with co-assembly partners affects a wide range of physical, chemical and biological properties, which leads to the formation of both ordered and disordered superstructures.<sup>[1]</sup> For instance, spherical nanoparticles functionalized with multiple charged ligands (also called superions) and nanoscale analogues of simple ions exhibit similar behaviours in several ways.<sup>[2]</sup> These oppositely charged ‘superions’ can co-assemble into binary nanoparticle crystals due to the electrostatic attractions and resemble the formation of salt crystals by oppositely charged ions.<sup>[2a, 3]</sup> Despite the extensive studies of the self-assembly of nanoparticles<sup>[4]</sup>, there is still critical information missing on the co-assembly of charged nanoparticles with oppositely charged ions, such as the effects of valency, shape and size of these superions. Very recently, Bian et al.<sup>[2c]</sup> reported that molecular ions with as few as three electric charges can co-assemble with oppositely charged nanoparticles and effectively induce attractions between charged nanoparticles in water. These interactions between molecular ions and nanoparticles can remarkably modulate the formation of colloidal crystals. The Classical Derjaguin-Landau-Verwey-Overbeek (DLVO) theory<sup>[5]</sup> divides the interactions between colloidal particles in solution into van der Waals (attractive) and the electrostatic (repulsive) as a function of separation distance.<sup>[6]</sup> The theory has been widely adopted for the explanations of colloidal stability and rationalization of the forces acting on colloidal particles. However, this theory is not readily applicable to charged nanoparticles due to the non-additivity of nanoparticle interactions on the nanoscale.<sup>[1a, 1b]</sup> In our study, a novel approach in the fabrication of nanoparticle superstructures has been utilized. The explored mechanism of interactions between molecular ions and nanoparticles offers several applications in nanoscale synthesis and engineering of nanoparticle superstructures.

Electrostatic interactions play a major role in the co-assembly of molecular ions and nanoparticles.<sup>[7]</sup> However, the detailed co-assembly mechanism of charged nanoparticles and oppositely charged molecular ions remain to be elucidated. Herein, we focused on probing the electrostatic co-assembly mechanisms of charged nanoparticles and oppositely charged molecular ions. The study depicts the effects of valency, shape and size of molecular ions on this co-assembly. Previously, Bian et al.<sup>[2c]</sup> reported the molecular dynamics simulations (MD) of trimethyl (mercaptoundecyl) ammonium (TMA)-coated gold nanoparticles (denoted as Au-TMA nanoparticles) and citrates using coarse-grained (CG) Martini 2 force field<sup>[8]</sup>. However, the methodology deployed was an implicit solvent method for the MD simulation. Such, implicit solvent models may not accurately calculate solvation and sufficiently describe the electrostatic interactions between Au-TMA nanoparticles and citrates.<sup>[9]</sup> In contrast, we adopted the new Martini 3 force field<sup>[10]</sup> and the corresponding water model. The explicit water environment is considered more accurate and realistic than the implicit solvent model for the depiction of electrostatic interactions.<sup>[9b, 11]</sup> Moreover, the Martini 3 force field shows significant improvements and offers broader applications over the Martini 2 force field.<sup>[10, 12]</sup>

In our study we performed coarse-grained molecular dynamics (CGMD) simulations of Au-TMA nanoparticles with a gold core diameter of 4.9 nm and phosphoric anions. We used a series of phosphoric anions with different valences for the depiction of co-assembly with Au-TMA nanoparticles. The anions used in the study included dihydrogen phosphate ( $P1^-$ ), hydrogen phosphate ( $P1^{-2}$ ), trimetaphosphate ( $P3^{-3}$ ), pyrophosphate ( $P2^{-4}$ ), tetrakisphosphate ( $P4^{-6}$ ) and hexametaphosphate ( $P6^{-6}$ ). These anions are denoted as  $Pn^m$ , where  $n$  is the number of phosphates and  $m$  is the net electrical charge. The previous study by Bian et al.<sup>[2c]</sup> suggests  $P3^{-3}$ ,  $P2^{-4}$  and  $P6^{-6}$  anions as effective candidates in mediating attractions between Au-TMA nanoparticles. We speculated that  $P3^{-3}$  and  $P2^{-4}$  anions are comparable, with the  $P3^{-3}$  anion having a slightly larger molecular size and lower charge density than the  $P2^{-4}$  anion. Moreover, the  $P4^{-6}$  anion was used as a reference to  $P6^{-6}$  due to its equal charge despite having a smaller molecular size. Similarly,  $P2^{-4}$  and  $P4^{-6}$  anions as linear molecular anions while  $P3^{-3}$  and  $P6^{-6}$  anions as ring-shaped. In our study, we mainly utilized  $P1^-$  and  $P1^{-2}$  anions due to their relatively low valences. The selection of these molecular anions was then followed by a systematic investigation of the effects of several parameters including valency, shape and size of these

molecular anions on their electrostatic co-assembly with Au-TMA nanoparticles. Moreover, the selected phosphoric anions are particularly interesting as they are related to the phosphoric acid backbone of the DNAs. Therefore, the co-assembly of phosphoric anions and gold nanoparticles in this study may serve as a motivation for designing the DNA-based nanostructures, such as DNA templates and DNA origami, for their co-assembly with the positively charged gold nanoparticles into highly ordered superstructures, as reported by previous experimental studies.<sup>[13]</sup>

Our results mainly suggest that  $P^{1-}$  and  $P^{1-2}$  anions with electric charges less than three may not mediate sufficient attractions between Au-TMA nanoparticles. However, molecular anions with higher electric charges (i.e.,  $P^{3-3}$ ,  $P^{2-4}$ ,  $P^{4-6}$  and  $P^{6-6}$ ) successfully induce the aggregations of Au-TMA nanoparticles. Furthermore, the size and shape of anions have great influences on the distribution and dynamics of adsorbed anions and the dynamics of nanoparticle aggregates. Our study emphasizes that the valency, shape and size of molecular anions are important factors in mediating attractions between the Au-TMA nanoparticles. These important findings also pave the way to provide future guidance for the design of DNA templates and DNA origami co-assembling with positively charged nanoparticles.

## 2 | RESULTS AND DISCUSSION

### 2.1 | Interactions between positively charged Au-TMA nanoparticles and molecular anions

Detailed models of Au-TMA nanoparticle and phosphoric anions are shown in Figure 1A and Figure 1B, respectively. The model-building methodology of Au-TMA nanoparticle and phosphoric anions are provided in the Supporting Information. To evaluate the potential interactions, we performed MD simulations of Au-TMA nanoparticles and a series of phosphoric anions. Initially, two Au-TMA nanoparticles and phosphoric anions were randomly distributed. Figure 1C shows the final structures of the  $P^{1-}$ ,  $P^{1-2}$ ,  $P^{3-3}$  and  $P^{2-4}$  systems after the MD simulations. The results show that the two Au-TMA nanoparticles stay separated from each other in the  $P^{1-}$  and  $P^{1-2}$  systems while clustered in the  $P^{3-3}$  and  $P^{2-4}$  systems (Figure 1C).

To quantitatively monitor the aggregations of Au-TMA nanoparticles, the centre-of-mass (COM) distance between the two gold cores were calculated for all these four systems. During the MD simulations, the distance between the nanoparticle fluctuated for the  $P^{1-}$  and  $P^{1-2}$  systems, indicating the presence of dominant electrostatic repulsions between the two Au-TMA nanoparticles (Figure 1D). In contrast, the two equally charged Au-TMA nanoparticles in the  $P^{3-3}$  and  $P^{2-4}$  systems agglomerated at  $\sim 850$  ns and  $\sim 50$  ns, respectively. The aggregates formed in both systems remained stable during the rest of the simulations maintaining a COM distance of  $\sim 8.5$  nm. This result showed that both  $P^{3-3}$  and  $P^{4-6}$  anions can mediate efficient attractions between Au-TMA nanoparticles and were consistent with previous experimental findings<sup>[2c]</sup>.

Since the attractions between Au-TMA nanoparticles are associated with negative charges in the interfaces, it is essential to compute the negative charge near the contact interface of the Au-TMA nanoparticles. We adopted a cutoff distance of 1.5 nm and counted the number of negative charges of the anions within a diameter of  $\sim 1.5$  nm around the two Au-TMA nanoparticles. Consistent with the fluctuations of inter-nanoparticle distance in the  $P^{1-}$  and the  $P^{1-2}$  systems (Figure 1D), the negative interface charge of the two analyzed systems also fluctuated with the charge number less than 40 (Figure 1E). Interestingly, the negative interface charges reached  $\sim 85$  for both the  $P^{3-3}$  and  $P^{4-6}$  systems after the aggregation of the two Au-TMA nanoparticles. This indicates that interfacial  $P^{3-3}$  and  $P^{4-6}$  anions produce close electrostatic attractions with the Au-TMA nanoparticles.

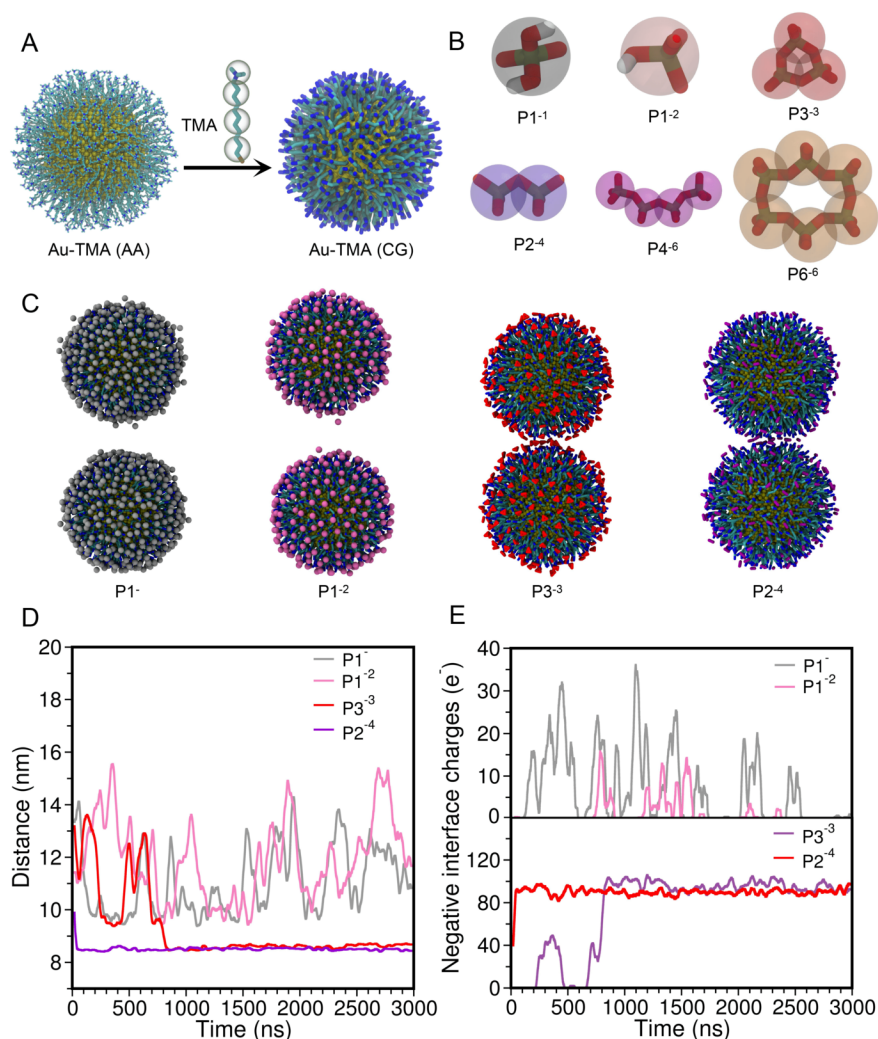


**FIGURE 1** MD simulations of Au-TMA nanoparticles and four molecular anions (P1<sup>-</sup>, P1<sup>-2</sup>, P3<sup>-3</sup> and P2<sup>-4</sup>). Demonstrating the all-atomic (AA) model of the Au-TMA nanoparticle with 384 TMA ligands (left panel), the mapping of the TMA ligand to four CG beads (middle panel) and a snapshot of the Martini CG model of the Au-TMA nanoparticle (right panel) (A). In the AA model of the Au-TMA nanoparticle, gold atoms are shown as yellow spheres and the TMA ligands are shown as sticks. Carbon, nitrogen and sulfur atoms are shown in cyan, blue and brown, respectively. Hydrogen atoms are omitted for clarity. In the CG model of the Au-TMA nanoparticle, the TMA ligands are represented by one positively charged bead and three neutral beads (also see Figure S4A), and the CG TMA ligands are shown as sticks. The positively charged bead is shown in blue while the other three neutral beads are shown in cyan. Martini mapping of P1<sup>-</sup>, P1<sup>-2</sup>, P3<sup>-3</sup>, P2<sup>-4</sup>, P4<sup>-6</sup> and P6<sup>-6</sup> anions is also presented (B). Whereas, the CG beads of P1<sup>-</sup>, P1<sup>-2</sup>, P3<sup>-3</sup>, P2<sup>-4</sup>, P4<sup>-6</sup> and P6<sup>-6</sup> anions are shown as semi-transparent grey, pink, red, purple, magenta and orange spheres, respectively. Final configurations of the P1<sup>-</sup>, P1<sup>-2</sup>, P3<sup>-3</sup> and P2<sup>-4</sup> systems (C). The P1<sup>-</sup> and the P1<sup>-2</sup> anions are shown in grey and pink spheres, respectively. The P3<sup>-3</sup> and P2<sup>-4</sup> anions are shown in red and purple sticks, respectively. All the anions within 1 nm distance from the Au-TMA nanoparticle surface is shown while sodium ions and water beads are not revealed for clarity. Time evolution of COM distances between Au-TMA nanoparticles for the four systems is also demonstrated (D) whereas the COM distance is measured by the COMs of the two gold cores. The time evolution of negative interface charge for the four

systems (E). The interface region defined in the demonstrations is measured as space within 1.5 nm around the two Au-TMA nanoparticles.

Next, we studied the co-assembly of Au-TMA nanoparticles with molecular anions featured with six negative charges (i.e.,  $P4^{-6}$  and  $P6^{-6}$ ). The previous analyses of Au-TMA nanoparticle aggregation in the  $P1^{-}$ ,  $P1^{-2}$ ,  $P3^{-3}$  and  $P2^{-4}$  systems were also performed in the  $P4^{-6}$  and  $P6^{-6}$  systems. Interestingly, the COM distance of the  $P4^{-6}$  system converged rapidly to  $\sim 8.5$  nm (Figure 2A) and was close to the results of the  $P2^{-4}$  and  $P3^{-3}$  systems (Figure 1D). However, the COM distance of the  $P6^{-6}$  system reached  $\sim 9.5$  nm at  $\sim 350$  ns and remained steadfast indicating stable aggregations of Au-TMA nanoparticles. Moreover, the final structures at the end of MD simulations demonstrated a close association between Au-TMA nanoparticles in  $P4^{-6}$  and relatively loose contacts of Au-TMA nanoparticles in the  $P6^{-6}$  systems (inset of Figure 2A). We speculate that this is due to the fact that  $P4^{-6}$  is a linear-shaped anion consisting of four beads while  $P6^{-6}$  is a ring-shaped anion with six beads. Therefore, the charge density of the  $P4^{-6}$  anion is higher than that of the  $P6^{-6}$  anion and contains fewer beads. Despite both the  $P4^{-6}$  and  $P6^{-6}$  anions having the same number of negative charges they still maintain differences in molecular shapes and sizes. This may be the main responsible factor for obtaining the different COM distances between Au-TMA nanoparticles (more discussion below).

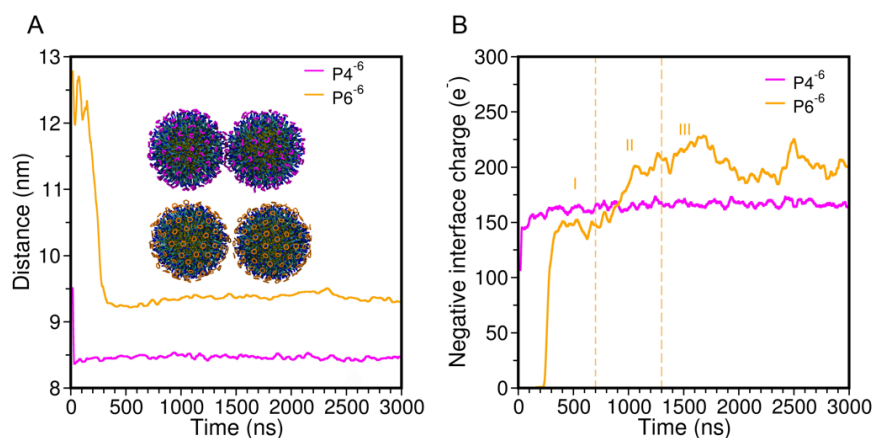


**FIGURE 2** MD simulations of Au-TMA nanoparticles and molecular anions featured six negative charges ( $P4^{-6}$  and  $P6^{-6}$ ). Time evolution of COM distance between Au-TMA nanoparticles in the  $P4^{-6}$  and  $P6^{-6}$  systems. Final configurations of  $P4^{-6}$  and  $P6^{-6}$  systems after MD simulations are also demonstrated. The  $P4^{-6}$  and  $P6^{-6}$  anions are shown in magenta and orange sticks, respectively. (A). Time evolution of negative interface charge for the  $P4^{-6}$  and  $P6^{-6}$  systems (B). The different Stages including *I*, *II* and *III* separated by orange dashed lines.

We further calculated the negative charges near the contact interface of the Au-TMA nanoparticles in  $P4^{-6}$  and  $P6^{-6}$  systems. Because of the slightly larger COM distance of Au-TMA nanoparticles in the  $P6^{-6}$  system than that of the  $P4^{-6}$  system (Figure 2A), we adopted a cutoff distance of 2 nm for the calculations of negative interface charges. The results show a rapid increase in the number of negative interface charges in the  $P4^{-6}$  system while remaining steady at  $\sim 150$ . This indicates that the equilibrium state is attained quickly after the aggregation of the two Au-TMA nanoparticles (Figure 2B). On the other hand, we observed that the number of negative interface charges as a function of time in the  $P6^{-6}$  system, could be divided into three stages. Stage *I* corresponds to the sharp increase to  $\sim 150$  charges during the first  $\sim 300$  ns and remaining steady until 700 ns. This first stage indicated the encounter of Au-TMA nanoparticles and the formation of a metastable state. However, the number of negative interface charges increased gradually to  $\sim 200$  until  $\sim 1300$  ns defining the stage *II* (from  $\sim 700$  ns to  $\sim 1300$  ns). This second stage is suggesting aggregation of  $P6^{-6}$  anions in the interfacial region. Finally, Stage *III* is considered as the equilibrium stage occurring after  $\sim 1300$  ns where the number of negative interface charges remained steady. All the representative snapshots

of these three stages are shown in Figure S8. Furthermore, higher negative interface charges in the P6<sup>-6</sup> system ( $\sim 200$ ) were observed as compared to the P4<sup>-6</sup> system ( $\sim 150$ ) during the final equilibrium stage. These results suggested the presence of stronger electrostatic attractions in the interfacial P6<sup>-6</sup> than those of the interfacial P4<sup>-6</sup> anions towards the Au-TMA nanoparticles.

These MD simulations predominantly revealed that the negatively charged phosphoric anions are attracted by the positively charged Au-TMA nanoparticles due to the presence of the electrostatic attractions. Meanwhile, anions diffuse more quickly than Au-TMA nanoparticles due to their significant smaller sizes. Moreover, the attained dynamic equilibrium of adsorption and desorption of anions on the Au-TMA nanoparticles is crucial. These anion densities near the Au-TMA nanoparticle surface play critical roles in mediating the aggregations of Au-TMA nanoparticles. The surface anion densities are influenced by the valency of molecular anion as it determines the electrostatic attraction strength with the positively charged Au-TMA nanoparticles according to Coulomb's law (more discussion below).

## 2.2 | Structural analysis of aggregates formed by Au-TMA nanoparticles and ions

Our results showed that P2<sup>-4</sup>, P3<sup>-3</sup>P4<sup>-6</sup> and P6<sup>-6</sup> anions can mediate effective aggregations of Au-TMA nanoparticles. We further evaluated the potentially important role of sodium ions in these aggregations. This was performed by comparing the positive interface charge which consisted of sodium ions in our four systems (Figure 3A). Our results suggested a higher number of interface charges of the P3<sup>-3</sup> system ( $\sim 16$ ) as compared to the positive interface charge of the P2<sup>-4</sup> system ( $\sim 8$ ). Interestingly, this observation with higher charges of P2<sup>-4</sup> than the P3<sup>-3</sup> anion indicated that the number of positive interface charges may correlate with the anion size and shape. Furthermore, we also found more ( $\sim 50$ ) cations in the interfacial regions of the P6<sup>-6</sup> system as compared to the P4<sup>-6</sup> system ( $\sim 24$ ) during the equilibrium stage (i.e., after  $\sim 300$  ns). This evidence further showed that the anion shape and size sustain influence on the interfacial ion distributions. Figure 3B shows the representative detailed snapshots of the interfacial regions of the P3<sup>-3</sup>, P2<sup>-4</sup>, P4<sup>-6</sup> and P6<sup>-6</sup> systems.

Similarly, the positive interface charge results were also consistent with the calculated COM distances of Au-TMA nanoparticles. The COM distances of Au-TMA nanoparticles during the aggregations were found comparable ( $\sim 8.5$  nm, see Figures 1C and 2B). This is in agreement with the smaller number of sodium ions in the interfacial regions for P3<sup>-3</sup>, P2<sup>-4</sup> and P4<sup>-6</sup> systems (Figure 4). Meanwhile, the COM distance of Au-TMA nanoparticles was relatively large ( $\sim 9.5$ nm, see Figure 2B) due to the significantly higher positive interface charge of the P6<sup>-6</sup> system (Figure 3).

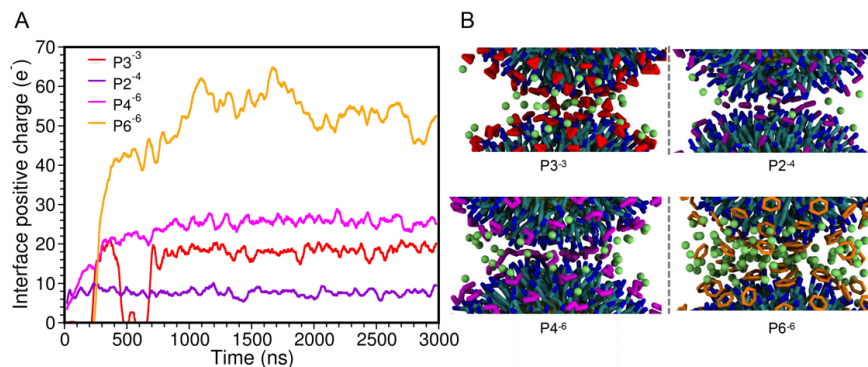


**FIGURE 3** The sodium cations in the interface regions of Au-TMA nanoparticles. The time evolution of positive interface charge for the P2<sup>-4</sup>, P3<sup>-3</sup> P4<sup>-6</sup> and P6<sup>-6</sup> systems (A). The contact interface region was demonstrated as space within a cutoff distance of 1.5 nm around the two Au-TMA nanoparticles. Snapshots of the detailed interface regions of the P2<sup>-4</sup>, P3<sup>-3</sup>, P4<sup>-6</sup> and P6<sup>-6</sup> systems (B). Whereas, the green spheres represent sodium ions.

In the next analysis, we systematically compared the electrostatic interactions in the aggregates by calculating the charge densities among the four tested systems. The charge distributions were calculated by summing the number of charges as a function of the distance from the surfaces of the two gold cores over the last 1500 ns of MD simulations. It is important to notice that the initial peaks of the charge density at  $\sim 1.5$  nm for the four systems correspond to the positive charges of TMA ligands (Figure 4A). During this analysis, the peak heights of  $P2^{-4}$  and  $P3^{-3}$  systems observed are lower than those of  $P4^{-6}$  and  $P6^{-6}$  systems which may be attributed to the smaller sizes of  $P2^{-4}$  and  $P3^{-3}$  anions. The smaller sizes of these anions also enabled them to partially penetrate the coating layer of TMA ligands and cause neutralization of the positive charges in these ligands.

As the positive charges of TMA ligands are further neutralized by the charges of anions, we also observed valleys for the charge density of these four systems. It can be described as charge reversal at the interface of Au-TMA nanoparticles. A detailed examination suggests that the valley positions are in the order of  $P2^{-4} < P3^{-3} < P4^{-6} < P6^{-6}$ , which can be attributed mainly to the increase in anion sizes. Meanwhile, the depths of the valleys are in the same order and correspond to an increase in negative charges near the surface of Au-TMA nanoparticles. It can be inferred that the electrostatic attractions between Au-TMA nanoparticles and surface anions are in the same order of  $P2^{-4} < P3^{-3} < P4^{-6} < P6^{-6}$ . Final snapshots of systems at the end of the MD simulation are demonstrated in Figure 4B. In comparison with the  $P2^{-4}$  and  $P3^{-3}$  systems, the  $P4^{-6}$  and  $P6^{-6}$  systems showed much fewer anions in the solutions, especially for the  $P6^{-6}$  system. This also employs that the molecular anions absorbed onto the Au-TMA nanoparticles reverse the surface charge from positive to negative and allow sodium ions further attracted towards the surface of Au-TMA nanoparticles. It is then followed by the appearance of second peaks representing charge accumulations observed at  $\sim 2.2$  nm. Interestingly, the heights of the second peaks were in the similar order of  $P2^{-4} < P3^{-3} < P4^{-6} < P6^{-6}$ . It also consistently indicates an order of electrostatic attractions between surface molecular anions and nearby cations.

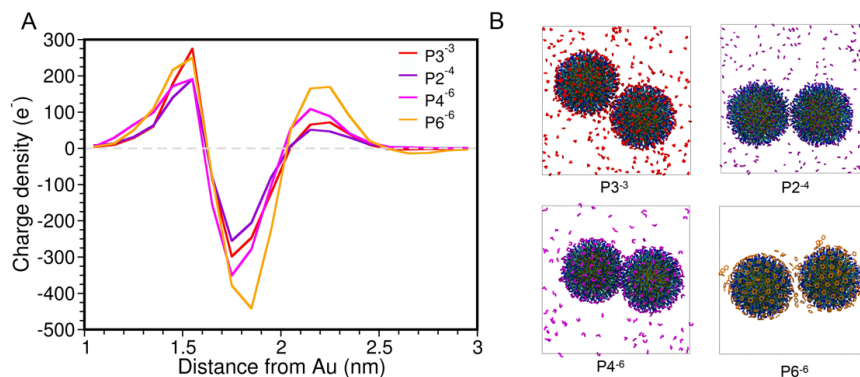


**FIGURE 4** The charge distribution of aggregates formed by Au-TMA nanoparticles and anions (A). The grey dashed line marks the position of zero net charge density. Snapshots of the final structure of the  $P2^{-4}$ ,  $P3^{-3}$ ,  $P4^{-6}$  and  $P6^{-6}$  systems (B). The simulation boxes are represented as black lines.

### 2.3 | Distributions and fluctuations of anions on the surface of Au-TMA nanoparticles

We analyzed the distribution of anions on the Au-TMA nanoparticles for the  $P2^{-4}$ ,  $P3^{-3}$ ,  $P4^{-6}$  and  $P6^{-6}$  systems. The symmetrical aggregates formed by the two Au-TMA nanoparticles were inspected by considering two variables (i.e.,  $DIST$  and  $Rmin$ ) as performed in a previous study<sup>[2c]</sup>. The analysis was aimed to characterize the positions of anions on the surface of Au-TMA nanoparticles. Herein, the two gold cores are denoted as  $I$  and  $II$ , respectively. The distribution of each anion on the Au-TMA nanoparticles was calculated by its distance to the COMs of the gold core  $I$  and  $II$  (denoted as  $Dist(I)$  and  $Dist(II)$ , respectively). The variables  $DIST$  and  $Rmin$  are defined as the absolute difference and minimum of  $Dist(I)$  and  $Dist(II)$ .

, respectively (Figure 5A). The variable *DIST* characterizes the anion positions on the two nanoparticles, whereas *Rmin* indicates the radial distance to the closer Au-TMA nanoparticle.

We calculated the probabilities of anions distributions on the Au-TMA nanoparticles in the P2<sup>-4</sup>, P3<sup>-3</sup>, P4<sup>-6</sup> and P6<sup>-6</sup> systems as a function of *DIST* and *Rmin* over the last 1500 ns of MD simulations. The probability of anions distribution was firstly normalized by the number of anions in each system. This was necessary because of the higher number of anions in the P3<sup>-3</sup> and P2<sup>-4</sup> systems than those in the P4<sup>-6</sup> and P6<sup>-6</sup> systems (see Table S4). We found that the P3<sup>-3</sup> anions were distributed mostly on the nanoparticle with *DIST* values greater than 2.5 nm while the P2<sup>-4</sup> anions were located mainly on the nanoparticle with *DIST* values greater than 3.5 nm (Figure 5B). Meanwhile, as compared to the *Rmin* distributions of the P3<sup>-3</sup> system, the *Rmin* distribution of the P2<sup>-4</sup> system was found wider with an obvious difference of  $Rmin \sim 4$ . This result implies TMA ligands specific higher penetration of P2<sup>-4</sup> anions in contrast to P3<sup>-3</sup> anions and may be contributed by the smaller size of P2<sup>-4</sup> anions. On the other hand, the distributions of P4<sup>-6</sup> and P6<sup>-6</sup> on the Au-TMA nanoparticles were denser. This is consistent with the previous finding of strong electrostatic interactions between anions featured with six negative charges and Au-TMA nanoparticles. Meanwhile, the distributions of P4<sup>-6</sup> and P6<sup>-6</sup> on the Au-TMA nanoparticles were found quite similar except for barely seen distributions of P6<sup>-6</sup> anions in proximity to the interface of the two nanoparticles (i.e., the *DIST* close to zero). This may be attributed to the larger COM distance of Au-TMA nanoparticles in the P6<sup>-6</sup> system and aggregation of the interface region with sodium ions and P6<sup>-6</sup> anions (see Figures 2B and 3B).

Furthermore, we characterized the anions into three classes based on its dynamics on the nanoparticles and in the solution. The anion in the solution was the first class subjected to this analysis (Figure 5C). Herein, we adopted a *DIST* criterion of 2 nm to further classify the two other classes of anions (interface and outer) on the nanoparticles based upon the anion distribution results (Figure 5B). Finally, the anions on the Au-TMA nanoparticle surfaces with *DIST* greater than 2.0 (pink) and *DIST* equal to or less than 2 nm (green) were classified as interface anions (the second class) while others as outer anions (the third class), respectively.

We further calculated the transition probabilities of these three regions during the last 1500 ns of MD simulations. We found that anions in the solutions and the outer regions were quite stable for all the four systems (Figure 5D). Notably, the anion transition between outer anions and interface anions in the P2<sup>-4</sup> system was more dynamic than that of the P3<sup>-3</sup> system. Similarly, the transition between outer anions and interface anions was more dynamic in the P4<sup>-6</sup> system than that in the P6<sup>-6</sup> system. Interestingly, close transition probabilities of outer anions and interface anions were observed for the P3<sup>-3</sup> and P4<sup>-6</sup> systems. These comparisons briefly summarize that the increase in anion charge mainly reduce the dynamics of anion transitions. In a similar way, the detailed analysis also employs that the ring structure and larger size of anions reduce the dynamics of anion transitions in contrast to the linear ones with smaller sizes.

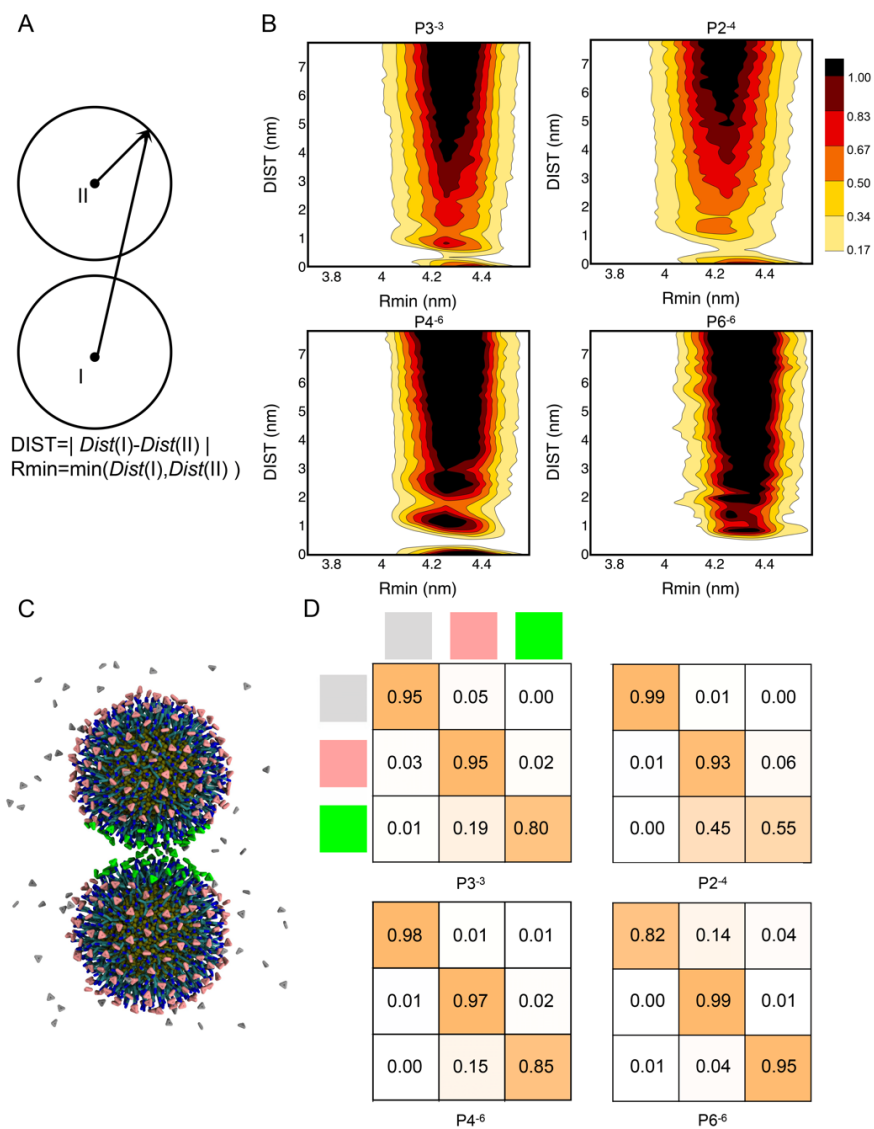


**FIGURE 5** The anions distribution on the Au-TMA nanoparticles and transition probability matrices. Scheme for the definitions of variables  $DIST$  and  $Rmin$  (A). The two gold cores are denoted as  $I$  and  $II$ , respectively. Whereas, each anion on the Au-TMA nanoparticles calculated by its distance to the COMs of gold core  $I$  and  $II$  are presented (denoted as  $Dist(I)$  and  $Dist(II)$ , respectively). The variables  $DIST$  and  $Rmin$  demonstrate the absolute difference and minimum of these  $Dist(I)$  and  $Dist(II)$ , respectively. The probabilities of anions distributions on the Au-TMA nanoparticles as a function of  $DIST$  and  $Rmin$  are also shown (B). The schematic representation of the three anion classes (C). Whereas, anions in the solutions belonging to the first class are shown in grey. The anions on the Au-TMA nanoparticle surfaces with  $DIST$  greater than 2.0 (shown as pink) and  $DIST$  equal to or less than 2 nm (shown as green) are classified into interface anions (the second class) and outer anions (the third class), respectively. The transition matrix of anions in the P2<sup>-4</sup>, P3<sup>-3</sup>, P4<sup>-6</sup> and P6<sup>-6</sup> systems with demonstrated transitions between the three regions obtained from the last 1500 ns of MD simulations (D). The grey, pink and red squares denote anions in the solution, outer anions and interface anions, respectively. Whereas, the sum of each vertical column equals one.

## 2.4 | Dynamics of Au-TMA nanoparticles

In our last analysis, we measured the effects of molecular anions on the dynamics of Au-TMA nanoparticles in these aggregates. This was performed by estimations of the relative rotation of two Au-TMA nanoparticles. Herein, the relative rotation of Au-TMA nanoparticles was calculated by using one Au-TMA nanoparticle as the reference. The analysis was performed over the last 1500 ns of MD simulations with a time interval of 4 ns (Figure 6A). In comparison with the rotation angle of the P2<sup>-4</sup> system, the rotation angle of the P3<sup>-3</sup> system was significantly smaller which indicated a more dynamic rotation of Au-TMA nanoparticles in the P2<sup>-4</sup> system (Figure 6B). This may be potentially contributed by the higher charge density and smaller anion size of the P2<sup>-4</sup> anion. On the other hand, the dynamics of the P2<sup>-4</sup> anions in the interface region were found higher than the interface of anions in the P3<sup>-3</sup> system (see Figure 5D). This may be attributed to a lower rotational barrier of Au-TMA nanoparticles in the P2<sup>-4</sup> systems than that of the P3<sup>-3</sup> system. However, the rotation angle of the P3<sup>-3</sup> system is close to that of the P4<sup>-6</sup> system. Interestingly, close proximity transition probabilities involving anions in the interface region for both P3<sup>-3</sup> and P4<sup>-6</sup> systems were also observed (see Figure 5D). The data infers that the linear-shaped P4<sup>-6</sup> anion with higher charge density matches the dynamics properties of the P3<sup>-3</sup> anion because of its stronger interaction with Au-TMA nanoparticles. Moreover, the rotation angle in the P6<sup>-6</sup> system was much smaller than that of the P4<sup>-6</sup> system and consistent with the transition probability of these two systems. We speculate that the interfacial aggregates formed by P6<sup>-6</sup> anions and sodium ions present a significant rotational barrier to the rotation of Au-TMA nanoparticles. We propose this effect to significantly reduce the dynamics of Au-TMA nanoparticles within the aggregate.

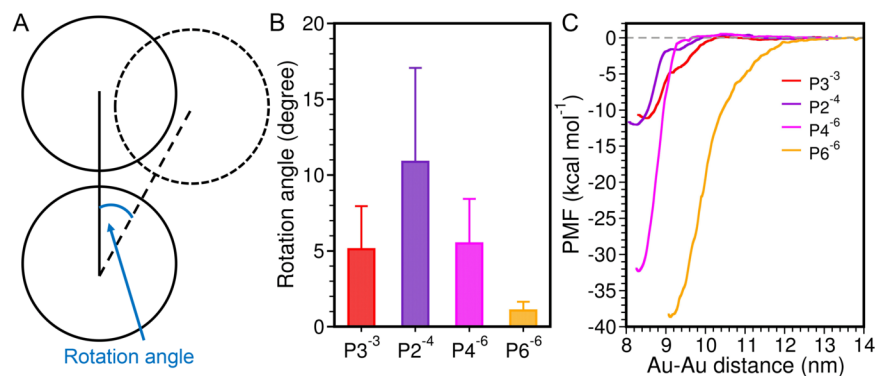


**FIGURE 6** Rotation angles of the two Au-TMA nanoparticles in the aggregates. Scheme for the definition of the rotation angle (A) and the results of rotation angles in the P2<sup>-4</sup>, P3<sup>-3</sup>, P4<sup>-6</sup> and P6<sup>-6</sup> systems calculated over the last 1500 ns of MD simulations (B). The time interval of the trajectories is 4 ns. The error bar denotes the standard deviations. The PMF profiles of P2<sup>-4</sup>, P3<sup>-3</sup>, P4<sup>-6</sup> and P6<sup>-6</sup> systems along the reaction coordinates were calculated as the distance between the COMs of the two gold cores of the Au-TMA nanoparticles (C).

Hence, the molecular anions play a significant role in mediating the aggregations of Au-TMA nanoparticles and are referred as “ionic glues”<sup>[14]</sup>. We further evaluated the interactions between the two Au-TMA nanoparticles by calculating the potential of mean force (PMF) profile. This was performed by analyzing the distance between the COMs of the two gold cores in the Au-TMA nanoparticles as the reaction coordinate. The results suggested a higher disassociation free energy barrier in the P4<sup>-6</sup> and P6<sup>-6</sup> systems as compared to the P3<sup>-3</sup> and P2<sup>-4</sup> systems. Specifically, the disassociation free energy barrier of P3<sup>-3</sup> was found slightly lower than that of P2<sup>-4</sup> system despite a higher electric charge (Figure 6C). In comparison, the PMF profile of the P6<sup>-6</sup> system showed a significantly larger disassociation free energy barrier than the P4<sup>-6</sup> system. These observations further emphasized the critical roles of the shape and size of these anions in mediating the aggregation of Au-TMA nanoparticles.

Based on the overall results, we speculate two folds effect of anion size and shape on these aggregations.

Notably, the effects of anion ring structures (P3<sup>-3</sup> and P6<sup>-6</sup>) are associated with their relative low configuration entropies. It may also serve as a major contributor in altering electrostatic interaction with Au-TMA nanoparticles and sodium ions. This effect resembles the configurational entropy loss, where the ligand is rigidified in the classic ligand-protein binding. This configuration entropy loss of ligand is favorable for its binding to protein<sup>[15]</sup>. On the other hand, the effects of molecular size can be interpreted as the distributed charges being superior to collected charges in adsorbing onto the Au-TMA nanoparticles. Molecular anions with more distributed charges (P3<sup>-3</sup> and P6<sup>-6</sup>) can adsorb efficiently onto Au-TMA nanoparticles. This infers stronger electrostatic interactions with Au-TMA nanoparticles (see Figure 4A) and further promotes the adhesions between Au-TMA nanoparticles.

### 3 | Conclusion

In this work, we mainly studied the effects of valency, shape and size of molecular anions on their co-assembly with the positively charged Au-TMA nanoparticles. The results of COM distance of gold cores showed that anions with charges greater or equal to three serve as effective “ionic glues”<sup>[14]</sup> to the Au-TMA nanoparticles in consistence with the previous experimental findings<sup>[2c]</sup>. Furthermore, the charge density calculations suggested that ring-structured P3<sup>-3</sup> anion with a larger size can more efficiently reverse the surface charge density from positive to negative and has a lower transition probability in the interface region as compared to the linear P2<sup>-4</sup> anion. Similar observations were evident from comparison of the linear P4<sup>-6</sup> anion and the ring-structured P6<sup>-6</sup> anion with a larger size. These findings suggested that ring structures and large sizes of the anions facilitates the interactions with Au-TMA nanoparticles and reduces the electrostatic repulsions between Au-TMA nanoparticles. Consistently, the PMF profiles revealed that the disassociation free energy tends to increase as anion valency increases. In our results, the P6<sup>-6</sup> system showed a significantly larger disassociation free energy barrier than the P4<sup>-6</sup> system. These findings suggested the critical roles of the shape and size of an anion in mediating the aggregation of Au-TMA nanoparticles. Furthermore, these Au-TMA nanoparticles in the P6<sup>-6</sup> system show relatively low rotational dynamics but higher dissociation free energy. However, aggregates are formed by sodium ions and P6<sup>-6</sup> anions in the highly curved interface regions of Au-TMA nanoparticles mediated by strong electrostatic attractions between sodium ions and P6<sup>-6</sup> anions. These observations mainly attribute to the combination of the high valency, ring structure and large size of P6<sup>-6</sup> anions. Our performed study emphasizes that the valency, shape and size of molecular anions are important factors in mediating attractions between the Au-TMA nanoparticles.

The potential future implication may be based on the P6<sup>-6</sup> system with augmented inter-particle distance due to increased ion size. This property may aid as a potential method to fine-tune the lattice parameters of electrostatic co-assembly formed by charged nanoparticles and oppositely charge molecular ions<sup>[16]</sup>. Furthermore, the phosphoric anions related to the phosphate backbones of DNA may also be useful. Previously, DNA and DNA origami have been widely adopted as templates in nanoparticle assembly or co-assembly with nanoparticle<sup>[17]</sup>. Therefore, designing DNA-based nanostructures, such as DNA templates and DNA origami, for their co-assembly with positively charged gold nanoparticles into highly ordered superstructures may be inspired by the findings of the current study.

### Acknowledgements

We thank Taimoor Khan, Damiano Buratto and Dong Zhang for their helpful discussions. This work was partially supported by the National Key Research and Development Program of China (2021YFA1201201, 2021YFF1200404), National Natural Science Foundation of China (Grants U1967217), National Independent Innovation Demonstration Zone Shanghai Zhangjiang Major Projects (ZJZX2020014), Starry Night Science Fund of Zhejiang University Shanghai Institute for Advanced Study (SN-ZJU-SIAS-003) and BirenTech Research (BR-ZJU-SIAS-001). R.Z. also acknowledges the financial support from W. M. Keck Foundation (Grant award 2019-2022).

### Conflict of Interests

The authors declare no conflict of interests.

## References

- [1] aA. Silvera Batista Carlos, G. Larson Ronald, A. Kotov Nicholas, *Science* **2015** , *350* , 1242477; bT. Hueckel, G. M. Hocky, J. Palacci, S. Sacanna, *Nature* **2020** , *580* , 487-490; cF. Matter, A. L. Luna, M. Niederberger, *Nano Today***2020** , *30* , 100827; dD. Luo, C. Yan, T. Wang, *Small***2015** , *11* , 5984-6008; eS. Hossain, D. Hirayama, A. Ikeda, M. Ishimi, S. Funaki, A. Samanta, T. Kawawaki, Y. Negishi, *Aggregate* **2022** , *n/a* , e255.
- [2] aM. Kalsin Alexander, M. Fialkowski, M. Paszewski, K. Smoukov Stoyan, J. M. Bishop Kyle, A. Grzybowski Bartosz, *Science***2006** , *312* , 420-424; bA. M. Kalsin, B. Kowalczyk, S. K. Smoukov, R. Klajn, B. A. Grzybowski, *J. Am. Chem. Soc.***2006** , *128* , 15046-15047; cT. Bian, A. Gardin, J. Gemen, L. Houben, C. Perego, B. Lee, N. Elad, Z. Chu, G. M. Pavan, R. Klajn, *Nat. Chem.* **2021** , *13* , 940-949; dY. Cao, S. Yang, Y. Li, J. Shi, *Aggregate* **2021** , *2* , e49.
- [3] aM. A. Boles, M. Engel, D. V. Talapin, *Chem. Rev.***2016** , *116* , 11220-11289; bK. He, Y. Jiang, T. Wang, Z. Liu, M. Wang, L. Pan, X. Chen, *Aggregate* **2022** , *3* , e57.
- [4] aB. Liu, X. Lu, Z. Qiao, L. Song, Q. Cheng, J. Zhang, A. Zhang, Y. Huang, T. Chen, *Langmuir* **2018** , *34* , 13047-13056; bQ. Cheng, L. Song, H. Lin, Y. Yang, Y. Huang, F. Su, T. Chen, *Langmuir* **2020** , *36* , 250-256; cH. Lin, L. Song, Y. Huang, Q. Cheng, Y. Yang, Z. Guo, F. Su, T. Chen, *ACS Appl. Mater. Interfaces* **2020** , *12* , 11296-11304; dL. Song, Y. Huang, Z. Nie, T. Chen, *Nanoscale* **2020** , *12* , 7433-7460.
- [5] Z. Adamczyk, P. Weroński, *Adv. Colloid Interface Sci.***1999** , *83* , 137-226.
- [6] C. J. van Oss, R. F. Giese, P. M. Costanzo, *Clays Clay Miner.* **1990** , *38* , 151-159.
- [7] aP. Y. Kim, J.-W. Oh, J.-M. Nam, *J. Am. Chem. Soc.***2015** , *137* , 8030-8033; bR. Platel, L. Vaure, E. Palleau, S. Raffy, F. Guérin, D. Lagarde, R. Cours, C. Marcelot, B. Warot-Fonrose, C. Nayral, F. Delpech, L. Ressler, *J. Colloid Interface Sci.* **2021** , *582* , 1243-1250.
- [8] S. J. Marrink, H. J. Risselada, S. Yefimov, D. P. Tieleman, A. H. de Vries, *J. Phys. Chem. B* **2007** , *111* , 7812-7824.
- [9] aD. P. Hua, H. Huang, A. Roy, C. B. Post, *Protein science : a publication of the Protein Society* **2016** , *25* , 204-218; bC. Arnarez, J. J. Uusitalo, M. F. Masman, H. I. Ingólfsson, D. H. de Jong, M. N. Melo, X. Periole, A. H. de Vries, S. J. Marrink, *J. Chem. Theory Comput.* **2015** , *11* , 260-275.
- [10] P. C. T. Souza, R. Alessandri, J. Barnoud, S. Thallmair, I. Faustino, F. Grünwald, I. Patmanidis, H. Abdizadeh, B. M. H. Bruininks, T. A. Wassenaar, P. C. Kroon, J. Melcr, V. Nieto, V. Corradi, H. M. Khan, J. Domański, M. Javanainen, H. Martinez-Seara, N. Reuter, R. B. Best, I. Vattulainen, L. Monticelli, X. Periole, D. P. Tieleman, A. H. de Vries, S. J. Marrink, *Nat. Meth.* **2021** , *18* , 382-388.
- [11] D. Bochicchio, G. M. Pavan, *The Journal of Physical Chemistry Letters* **2017** , *8* , 3813-3819.
- [12] aR. Alessandri, J. Barnoud, A. S. Gertsen, I. Patmanidis, A. H. de Vries, P. C. T. Souza, S. J. Marrink, *Advanced Theory and Simulations* **2022** , *5* , 2100391; bF. Grünwald, R. Alessandri, P. C. Kroon, L. Monticelli, P. C. T. Souza, S. J. Marrink, *Nat. Commun.* **2022** , *13* , 68.
- [13] aS. Julin, A. Korpi, Nonappa, B. Shen, V. Liljeström, O. Ikkala, A. Keller, V. Linko, M. A. Kostiainen, *Nanoscale***2019** , *11* , 4546-4551; bV. Linko, M. A. Kostiainen, *Nat. Mater.* **2020** , *19* , 706-707; cY. Tian, J. R. Lhermitte, L. Bai, T. Vo, H. L. Xin, H. Li, R. Li, M. Fukuto, K. G. Yager, J. S. Kahn, Y. Xiong, B. Minevich, S. K. Kumar, O. Gang, *Nat. Mater.* **2020** , *19* , 789-796.
- [14] T. Kraus, *Nat. Chem.* **2021** , *13* , 925-926.
- [15] aW. You, Y.-m. M. Huang, S. Kizhake, A. Natarajan, C.-e. A. Chang, *PLoS Comput. Biol.* **2016** , *12* , e1005057; bA. Chang Chia-en, W. Chen, K. Gilson Michael, *Proceedings of the National Academy of Sciences* **2007** , *104* , 1534-1539.

[16] V. Liljeström, J. Seitsonen, M. A. Kostainen, *ACS Nano***2015** , 9 , 11278-11285.

[17] aJ. A. Johnson, A. Dehankar, J. O. Winter, C. E. Castro, *Nano Lett.* **2019** , 19 , 8469-8475; bZ. Xue, C. Yan, T. Wang, *Adv. Funct. Mater.* **2019** , 29 , 1807658; cW. Zhou, Q.-Y. Lin, J. A. Mason, V. P. Dravid, C. A. Mirkin, *Small* **2018** , 14 , 1802742; dS. Julin, S. Nummelin, M. A. Kostainen, V. Linko, *Journal of Nanoparticle Research***2018** , 20 , 119.